IOPscience iopscience.iop.org

Home Search Collections Journals About Contact us My IOPscience

Numerical simulation of the transient photoconductivity in hydrogenated amorphous silicon including localized-state electron hopping

This article has been downloaded from IOPscience. Please scroll down to see the full text article.

2007 J. Phys.: Condens. Matter 19 436220

(http://iopscience.iop.org/0953-8984/19/43/436220)

View the table of contents for this issue, or go to the journal homepage for more

Download details:
IP Address: 129.252.86.83
The article was downloaded on 29/05/2010 at 06:20

Please note that terms and conditions apply.

J. Phys.: Condens. Matter **19** (2007) 436220 (12pp) doi:10.1088/0953-8984/19/43/436220

Numerical simulation of the transient photoconductivity in hydrogenated amorphous silicon including localized-state electron hopping

S Tobbeche[1] **and A Merazga**[2]

[1] Department of Electronics, Faculty of Science and Engineering, University Mohammed Khieder, PO Box 145, Biskra 07000, Algeria
[2] Department of Physics, Faculty of Science, King Khalid University, PO Box 9004, Abha, Saudi Arabia

E-mail: souad_tobbeche@yahoo.fr

Received 4 April 2007, in final form 30 May 2007
Published 1 October 2007
Online at stacks.iop.org/JPhysCM/19/436220

Abstract
The transient photoconductivity (TPC) in hydrogenated amorphous silicon is studied by numerical simulation. In addition to normal free carrier capture (emission) transitions into (from) localized states by the multiple-trapping (MT) process, we include the process of electron hopping (EH) through the conduction band tail states. The distribution of the dangling bond density is calculated by the defect pool model, while exponential distributions are assumed for the conduction and valence band tails. The simulation results are in good agreement with previous theoretical results: a hopping transport energy level identified as the peak of the energy distribution of the hopping photoconductivity is in excellent agreement with the theoretical hopping transport energy of Monroe. The simulated TPC is studied as a function of temperature in order to determine the relative contribution of MT and EH transport mechanisms. A smooth transition around 130 K between high temperature extended-state conduction via MT and low temperature localized-state EH is determined.

1. Introduction

Hydrogenated amorphous silicon (a-Si:H) can be doped effectively [1, 2], and this property has attracted considerable interest and research effort as well as applications in large-area electronics, solar cells and thin film transistors. The electronic properties of a-Si:H are dominated by carrier interactions with the disorder induced density of localized band tail states in the gap adjacent to the conduction and valence bands. The mechanisms of carrier transport depend sensitively on the temperature and the density of localized states. At sufficiently high

 © 2007 IOP Publishing Ltd Printed in the UK

temperatures and/or low density of localized states, the carriers move in the bands of extended states. When the temperature is sufficiently low and/or the density of localized states is high, the transport is controlled by hopping in the distribution of localized states.

Near room temperature, the results of the transient photo-response measurements in a-Si:H are well described by the multiple-trapping (MT) model [3, 4], in which the free carriers created by the short laser pulse move by continuous trapping and release into and from localized tail states. The interpretation of the MT process was obtained by describing the evolution of the carriers in terms of a time-dependent demarcation energy. At low temperatures, Monroe [5] analyzed the transient carrier thermalization by hopping between localized states in an exponential band tail. Marschall has studied by simulation the transient photocurrent (TPC) in disordered semiconductors in the case of hopping transport using Monte Carlo techniques [6]. Main *et al* [7] have also simulated the TPC in disordered semiconductors, including both MT and electron hopping (EH) processes, using a matrix-based Markov chain computation.

The present paper extends our previous work on the steady state photo-transport in a-Si:H including EH through tail states, where a smooth transition around 110 K was drawn between low temperature EH transport in the conduction band tail (CBT) and high temperature extended-state transport [8]. Similarly, the purpose of the present work is to provide numerical simulations for the TPC in undoped a-Si:H, involving both conduction mechanisms related to extended states via MT and localized-state EH, and determine the relative contribution of each with varying temperature. We consider an exponential CBT and a valence band tail (VBT) and use the defect pool model (DPM) for the dangling bond (DB) defect density [9, 10]. The resulting density of states with three components of different state types (the valence band donor-like tail states, the conduction band acceptor-like tail states and the DPM-DB states) is then used to simulate the TPC. We follow the numerical method applied by Main *et al* [7] in modeling the TPC with coupled MT and EH transport. This method consists of dividing the energy gap into closely spaced energy levels and solving simultaneously in the transient regime coupled rate equations corresponding to each energy level, for all free and trapped carrier densities. The simulations cover low and high temperatures in a single model that couples localized–extended and localized–localized state carrier transitions. The results are in close agreement with Monroe analysis of hopping transport at low temperatures. The effect of the temperature on the two conduction mechanisms shows a significant contribution of the EH process at low temperatures ($T < 130$ K), while the MT mechanism becomes dominant at moderate and high temperatures ($T > 130$ K).

2. TPC simulation

The density of states distribution of the intrinsic a-Si:H chosen for the present work (figure 1) includes exponential CBT and VBT:

$$g_c(E) = G_c \exp\left(\frac{E - E_c}{k_B T_c}\right) \qquad \text{and} \qquad g_v(E) = G_v \exp\left(\frac{E_v - E}{k_B T_v}\right) \tag{1}$$

with k_B the Boltzmann constant, E_c and E_v the mobility edges and the tail parameters, $T_c = 310$ K, $T_v = 550$ K, $G_c = 2 \times 10^{21}$ cm^{-3} eV^{-1} and $G_v = 2 \times 10^{21}$ cm^{-3} eV^{1} as model values chosen in agreement with the literature. The DB state distribution is calculated by the DPM [9, 10]:

$$D(E) = \xi \left(\frac{2}{f^0(E)}\right)^{k_B T^*/2E_{vo}} P\left(E + \frac{\sigma^2}{2E_{vo}}\right) \tag{2}$$

with

$$\xi = \left(\frac{G_v 2E_{vo}^2}{(2E_{vo} - k_B T^*)}\right)\left(\frac{H}{N_{SiSi}}\right)^{k_B T^*/4E_{vo}} \exp\left(\frac{-1}{2E_{vo}}\left(E_P - E_v - \frac{\sigma^2}{4E_{vo}}\right)\right),$$

and $P(E)$ is the Gaussian shaped defect pool with σ and E_p respectively its width and peak position in the gap. $E_{vo} = k_B T_v$ is the width of the VBT. H and N_{SiSi} are the total hydrogen and silicon concentrations, respectively, and T^* is the equilibrium temperature (freeze-in temperature). The density distributions of the different charge DB states (neutral or singly

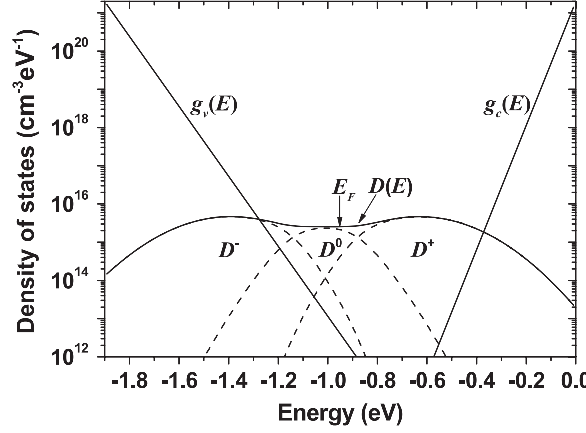

Figure 1. Density of states for undoped a-Si:H ($E_F = -0.9$ eV). Also shown are the exponential CBT, $g_c(E)$, and VBT, $g_v(E)$, state distributions and the total DB defect state distribution, $D(E)$, calculated by the DPM. The three components $D^-(E)$, $D^0(E)$, and $D^+(E)$ are shown in dashed lines.

occupied D^0 states, positively charged or unoccupied D^+ states, and negatively charged or doubly occupied D^- states) are given by

$$D^0(E) = D(E) f^0(E) \quad (3)$$

$$D^+(E) = D(E) f^+(E) \quad (4)$$

$$D^-(E) = D(E) f^-(E) \quad (5)$$

with f^0, f^+ and f^- the thermal equilibrium DB occupation functions [11], the probabilities for the DB state of being, respectively, singly occupied, unoccupied, and doubly occupied. The arrow in figure 1 points to the dark Fermi energy, E_F, positioned at 0.9 eV below E_c, determined by solving the charge neutrality equation. This charge neutrality condition is verified at each instant throughout the simulation. The parameters used for the band tails and the DPM calculation of the DB density of states are given in table 1.

The simulation procedures are exactly those detailed in our paper on the steady state photo-response [8], except that the time-dependent densities of free and trapped carriers in the transient regime require a time-step definition in the applied finite difference technique [12] before applying the appropriate numerical method for the solution. The equations of the time-dependent carrier density rates are two continuity equations for the free carrier densities n and p at E_c and E_v,

$$\frac{dn}{dt} = \sum_i Re^n_{T,i} + Re^n_{D,i} - \sum_i Rc^n_{T,i} + Rc^n_{D,i} \quad (6a)$$

$$\frac{dp}{dt} = \sum_i Re^p_{T,i} + Re^p_{D,i} - \sum_i Rc^p_{T,i} + Rc^p_{D,i} \quad (6b)$$

Table 1. Parameters for the gap density of states.

E_g (eV)	1.9
G_v (cm^{-3} eV^{-1})	2×10^{21}
T_v (K)	550
σ (eV)	0.19
$E_c - E_p$ (eV)	0.63
E_{vo} (meV)	47.4
N_{SiSi} (cm^{-3})	2×10^{23}
H (cm^{-3})	5×10^{21}
U (eV)	0.2
T^* (K)	500
G_c (cm^{-3} eV^{-1})	2×10^{21}
T_c (K)	310

and $4N$ detailed balance equations, at each trap level of the N energy levels E_i ($i = 1, \ldots, N$) across the gap, for $4N$ trapped carrier densities, n_i (trapped electrons in CBT), p_i (trapped holes in VBT), N_i^+ (hole-occupied D^0 state), and N_i^- (electron-occupied D^0 state),

$$\frac{\mathrm{d}n_i}{\mathrm{d}t} = Rc_{T,i}^{n} - Re_{T,i}^{n} + R_{hi,i}^{n} - R_{\mathrm{ho},i}^{n}, \tag{7a}$$

$$\frac{\mathrm{d}p_i}{\mathrm{d}t} = Rc_{T,i}^{p} - Re_{T,i}^{p}, \tag{7b}$$

$$\frac{\mathrm{d}N_i^+}{\mathrm{d}t} = Rc_{D,i}^{n} - Re_{D,i}^{n}, \tag{8a}$$

$$\frac{\mathrm{d}N_i^-}{\mathrm{d}t} = Rc_{D,i}^{p} - Re_{D,i}^{p}. \tag{8b}$$

The carrier densities obtained by solving the $4N + 2$ coupled non-linear equations using appropriate numerical methods must satisfy the charge neutrality equation:

$$p + \sum_i p_i + \sum_i N_i^+ - n - \sum_i n_i - \sum_i N_i^- = 0 \tag{9}$$

at all time points over the simulation time range.

The MT rates $Rc_{T/D,i}^{n/p}$ and $Re_{T/D,i}^{n/p}$, associated with electron/hole capture/emission into/from tail/defect state at level E_i, have often been used in conventional TPC simulations that neglect hopping transitions [12, 13]. The EH rates $R_{hi,i}^{n}$ and $R_{\mathrm{ho},i}^{n}$, concerning the trapped electron density n_i associated with EH into (out of) CBT states at E_i, are expressed in terms of the nearest neighbor hopping theory in amorphous semiconductors [14]. The transport, in this approach, is based on the single hopping transition from level E_i to level E_j with the rate [15–17]

$$\Gamma_{i,j} = \nu_0 \left(\frac{g_c(E_j)}{G_T} \right) \times \exp\left(-\frac{2R_{i,j}}{a} \right) \qquad \text{if } E_i \geqslant E_j \text{ (iso-energetic or downward hops)} \tag{10a}$$

with $G_T = \int_{E_v}^{E_i} g_c(E)\, \mathrm{d}E$, the total density of CBT states deeper than E_i, or

$$\Gamma_{i,j} = \nu_0 \left(\frac{g_c(E_i)}{G_T} \right) \times \exp\left(-\frac{2R_{i,j}}{a} \right) \times \exp\left(-\frac{E_j - E_i}{k_B T} \right) \qquad \text{if } E_i < E_j \text{ (upward hops),} \tag{10b}$$

with $G_T = \int_{E_v}^{E_j} g_c(E)\,dE$ the total density of CBT states deeper than E_j. ν_0 is the attempt to escape frequency and a is the localization radius. $g_c(E_j)/G_T$ in equation (10*a*) and $g_c(E_i)/G_T$ in equation (10*b*) are respectively the weighting factors for the hopping probability to a state at $E_j \leqslant E_i$ and to a state at $E_j > E_i$. $R_{i,j}$ is the hopping distance from a state at E_i to a neighboring state at E_j, given by [6, 15, 16]

$$R_{i,j} = \{(4\pi/3)G_T\}^{-1/3} \tag{11}$$

with G_T, as above, having the integral expression depending on whether hopping from E_i is iso-energetic or downward, or it is upward. The total hopping rate out of level E_i is $R^n_{\mathrm{ho},i} = n_i \times \sum_j \Gamma_{i,j}$ and the EH photoconductivity at level E_i, taking account of Einstein relation [14], is

$$\sigma_{\mathrm{hop}}(E_i) = \frac{e^2}{6k_B T}(R_{i,j})^2 R^n_{\mathrm{ho},i}. \tag{12}$$

The total EH photoconductivity is then

$$\sigma_{\mathrm{hop}} = \frac{e^2}{6k_B T}\sum_i (R_{i,j})^2 R^n_{\mathrm{ho},i}. \tag{13}$$

The free electron and hole densities contribute to the TPC via MT following the expression

$$\sigma_{\mathrm{MT}}(t) = e[\mu_n n(t) + \mu_p p(t)] \tag{14}$$

where μ_n (μ_p) is the free electron (hole) mobility and e the electron charge. The total TPC is simply the sum of EH and MT photoconductivity components,

$$\sigma_{\mathrm{ph}}(t) = \sigma_{\mathrm{hop}}(t) + \sigma_{\mathrm{MT}}(t). \tag{15}$$

Table 2 lists the parameter values used in the TPC simulations.

Table 2. Parameters for the TPC simulation.

Parameter	Value
$N_c = N_v$ (cm^{-3})	10^{20}
$C_n^o = C_p^o$ (cm^3 s^{-1})	8.5×10^{-8}
$C_n^+ = C_p^-$ (cm^3 s^{-1})	3×10^{-7}
$C_n^c = C_p^v$ (cm^3 s^{-1})	5×10^{-8}
$C_p^c = C_n^v$ (cm^3 s^{-1})	5×10^{-9}
μ_n (cm^2 s^{-1} V^{-1})	10
μ_p (cm^2 s^{-1} V^{-1})	0.3
ν_0 (s^{-1})	2×10^{12}
a (cm)	5×10^{-7}

3. Results and discussion

Before dealing with the interpretation of the TPC results, we start by examining the influence of EH as coupled to the MT process. Figure 2 illustrates the relative contribution of EH to the TPC, where the TPC σ_{ph} (curve with symbol ○) is plotted together with the conventional TPC σ_{conv} uniquely based on MT (curve with symbol $*$). σ_{conv} is a result of a TPC simulation performed without the hopping terms in the rate equation (7*a*) [13] and is given by a similar equation to (14). We also show the two TPC components, due to MT conduction σ_{MT} (curve with symbol +) and to EH conduction σ_{hop} (curve with symbol △), to examine the relative contribution of each. The comparison is made for an excitation density $N = 10^{16}$ cm^{-3} at $T = 90$ K. It is clear that the TPC is dominated by the EH photoconductivity ($\sigma_{\mathrm{ph}} = \sigma_{\mathrm{hop}}$)

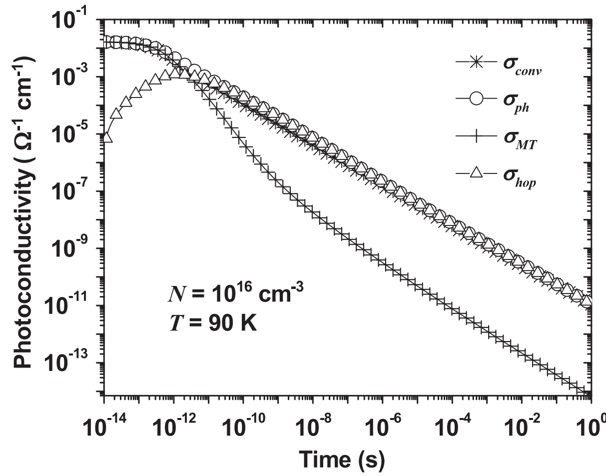

Figure 2. The MT photoconductivity $\sigma_{\rm MT}$ (symbol +) and EH photoconductivity $\sigma_{\rm hop}$ (symbol △) components of the TPC $\sigma_{\rm ph}$ (symbol O), at $T = 90$ K. The conventional TPC $\sigma_{\rm conv}$ (symbol ∗) simulated without EH consideration is also shown for comparison.

over the time range starting from $t = 5 \times 10^{-12}$ s. It is also clear that the new TPC $\sigma_{\rm ph}$ and the conventional TPC $\sigma_{\rm conv}$ are nearly superimposed over the entire time range (10^{-14}–1 s). Although the EH component $\sigma_{\rm hop}$ dominates the transport above $t = 5 \times 10^{-12}$ s (the onset time of electron trapping) and the MT component is negligibly low in this range, the EH process does not have a significant influence on the shape and magnitude of the conventional TPC $\sigma_{\rm conv}$. This leads to the conclusion that the TPC due to EH transport ($\sigma_{\rm hop}$) and that based uniquely on MT ($\sigma_{\rm conv}$) are similar for an exponential CBT. This result agrees with the simulation result of Silver *et al* [18] and Marshall *et al* [19] using Monte Carlo techniques. The TPC starts nearly constant owing to the carriers initially located in the extended states. After about 6×10^{-13} s, the TPC decreases following the power-law time dependence $\sigma_{\rm ph} \propto t^{-(1-\alpha_{\rm c})}$, where $\alpha_{\rm c} = T/T_{\rm c} = 0.29$ is the dispersion parameter. The behavior of $\sigma_{\rm ph}$ (dominated by $\sigma_{\rm hop}$) is similar to that of $\sigma_{\rm conv}$ for an exponential band tail [3, 4].

Now, we will study the electron thermalization by combined MT and EH transport. Before that, we will first recall the conventional electron thermalization occurring only via MT. Figure 3 shows the evolution of the energy distribution of trapped electron density n_i in the CBT at times from 10^{-14} to 1 s varying by a factor of 10 step. After excitation there is photogeneration of charge carriers, and after a very short time the electrons are in multiple interaction with the traps of the CBT. The progressive electron thermalization proceeds in the form of a packet. The majority of electrons are concentrated in the states around the demarcation energy $E_{\rm d}^{\rm conv}$, associated with the peak of the distribution, which moves with time deeper and deeper into the gap. The electrons located in the upper part of the packet ($E > E_{\rm d}^{\rm conv}$) are in thermal equilibrium with the free electrons of the conduction band and their density is $g_{\rm c}(E) \times f(E)$, with $f(E)$ the Boltzmann occupation function. In the lower part of the packet ($E < E_{\rm d}^{\rm conv}$) the electrons are distributed in parallel to the CBT. The conduction is controlled by electron capture and emission and the transport occurs through the extended states at $E_{\rm c}$. Figure 4 shows the energy distribution of the electron density n_i at times from 10^{-14} to 1 s, varying by a factor of 10 step, in the case where EH is coupled to MT. After the initial trapping of electrons, they are distributed in parallel to the CBT. The electrons initially located in the shallow states of high density move to lower energy levels by downward hopping.

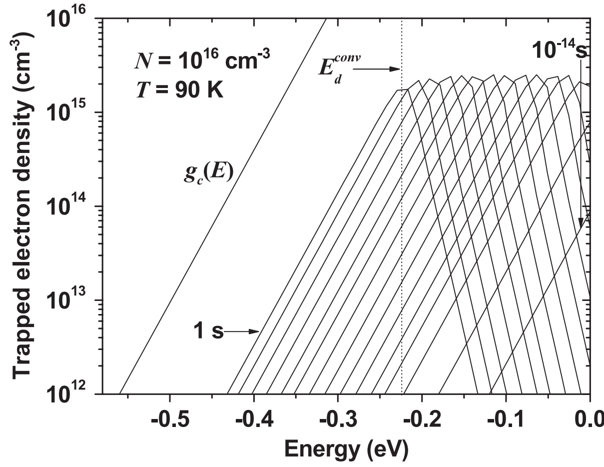

Figure 3. Energy distribution of the trapped electron density n_i, in the conventional case without EH consideration, for times ranging from 10^{-14} to 1 s with a factor of 10 step and at $T = 90$ K. The conventional demarcation energy $E_{\mathrm{d}}^{\mathrm{conv}}$ defined as the distribution peak is indicated.

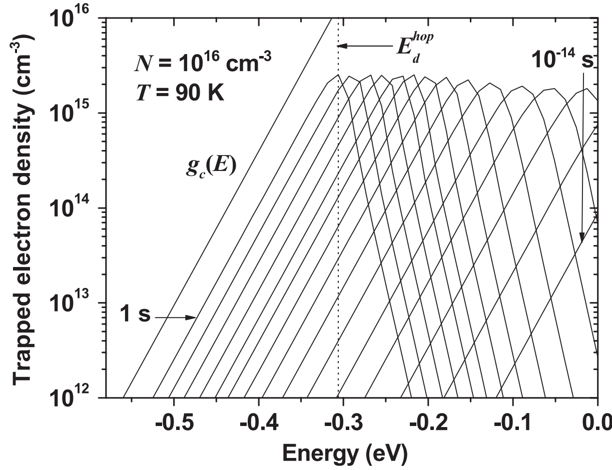

Figure 4. Energy distribution of the trapped electron density n_i, in the new case with EH consideration, for times ranging from 10^{-14} to 1 s with a factor of 10 step and at $T = 90$ K. The demarcation energy $E_{\mathrm{d}}^{\mathrm{hop}}$ defined by the distribution peak is indicated.

This is due to the fact that the downward hopping rate expressed by equation (10*a*) dominates at high density of states since the overlap term $\exp(-\frac{2R_{i,j}}{a})$ is high. The electrons will then hop down to deeper states and subsequently accumulate at a certain energy depth where the state density is low enough to prevent more downward hopping. During this thermalization, the majority of electrons are concentrated in the states around the charge distribution peak that represents the new demarcation level $E_{\mathrm{d}}^{\mathrm{hop}}$ which moves deeper into the gap with time. According to Monroe [5], the demarcation level is defined as the energy at which the typical downward hopping rate Γ_{typ} is equal to the reciprocal of the elapsed time following the excess carrier generation. Γ_{typ} is given by the equation

$$\Gamma_{\mathrm{typ}} = \nu_0 \exp[-2a^{-1}(k_{\mathrm{B}}T_{\mathrm{c}}G_{\mathrm{c}})^{-1/3} \exp(-E/3k_{\mathrm{B}}T_{\mathrm{c}})] \qquad (16)$$

and the demarcation energy at which $\Gamma_{\rm typ}(E)t = 1$ is

$$E_{\rm d} = k_{\rm B}T_{\rm c}\ln(8a^{-3}/(k_{\rm B}T_{\rm c}G_{\rm c})) - 3k_{\rm B}T_{\rm c}\ln[\ln(\nu_0 t)]. \tag{17}$$

Equation (17) is applied in the case of downward hopping for $t < [\tau_{\rm s} = \nu_0^{-1}\exp(3T_{\rm c}/T)]$. Monroe suggested that the thermalization must be dominated by the downward hopping process until the time $\tau_{\rm s}$, called the time of segregation. For $t > \tau_{\rm s}$, the majority of electrons are concentrated around a thermalization energy given by the expression

$$E_{\rm th} = -k_{\rm B}T\ln(\nu_{\rm typ}t) \tag{18}$$

where the typical hopping frequency $\nu_{\rm typ} = \tau_{\rm s}^{-1}\exp(-E_{\rm t}/k_{\rm B}T)$ is associated with upward hopping to a dominant hopping transport path, analogous to the mobility edge $E_{\rm c}$. Monroe stated that this path is centered at the transport level $E_{\rm t}$ defined by

$$E_{\rm t} = k_{\rm B}T_{\rm c}\ln(8a^{-3}/(27k_{\rm B}T_{\rm c}G_{\rm c})) - 3k_{\rm B}T_{\rm c}\ln(T_{\rm c}/T). \tag{19}$$

As $E_{\rm d}$ advances deeper into the gap, the downward hopping rate decreases because the exponential density of states decreases quickly with energy. Consequently, it becomes increasingly hard for the electron to find a close neighbor state to hop to. After a certain time, it becomes favorable for electrons to hop up in energy and so there is an increase of the number of states available for thermalization. Further thermalization then occurs by the hopping process. In this case, the thermalization energy $E_{\rm th}$ sinks into the gap following equation (18). At long times, electrons in deep states are thermally excited to the transport level $E_{\rm t}$ at which the variation of the overlap term in equation (10*b*) becomes too small to compete with the Boltzmann factor in the same equation. The transport is ensured by the hopping process and the dominated conduction is through the states located around the transport level $E_{\rm t}$. We can therefore summarize the EH transport as follows: at short times, the electrons are in shallow states and move by hopping down to lower energies. When they reach $E_{\rm t}$, it will happen that further hopping down to states below $E_{\rm t}$ is soon followed by electron upward hopping to $E_{\rm t}$. The EH process near $E_{\rm t}$ is similar to MT transport where electrons are activated to the mobility edge $E_{\rm c}$, and $E_{\rm t}$ is a transport path similar to $E_{\rm c}$. The development of such a dominant conduction path within localized states is shown in figure 5. This illustrates the energy distribution of the hopping photoconductivity $\sigma_{\rm hop}(E)$ given by equation (12) at times ranging from 10^{-14} to 10^4 s with a factor of 10 step. A conduction path is identified around the peak of each distribution, which shifts to deeper states for $t \leqslant 10^{-5}$ s. This behavior of the photoconductivity corresponds to the initial downward hopping regime. Afterwards, the peak stops shifting at the transport energy -0.17 eV below $E_{\rm c}$. This is clarified in figure 6, where we plot the photoconductivity distribution peak as a function of time. There is a transition time at about 10^{-5} s, after which the peak stops shifting down and stays close to -0.17 eV. The curve contains a *dip* feature at about 10^{-5} s (indicated by the arrow) just before it levels out at the energy -0.17 eV to indicate no more shift of the distribution peak beyond this level. This feature is also obtained by Main *et al* [7] in their TPC simulation dealing with combined MT and EH transport in disordered semiconductors. Indeed, as predicted by Monroe analysis, the transport energy calculated using equation (19) is at 0.18 eV below $E_{\rm c}$, which is in reasonable agreement with the result of our simulations and the simulations of Main *et al* [7].

In figure 7, the demarcation energy $E_{\rm d}^{\rm hop}$ (transport with EH) and the demarcation energy $E_{\rm d}^{\rm conv}$ (transport without EH) are plotted together as functions of time (curves with symbol □ and symbol ○, respectively). The equivalent results of Monroe are also shown for comparison: the $E_{\rm d}^{\rm hop}$-equivalent curve obtained by using equation (17) for up to the time $\tau_{\rm s}$ and equation (18) thereafter (curve with symbol ■) and the $E_{\rm d}^{\rm conv}$-equivalent curve obtained by simply using the conventional MT relation $E_{\rm th} = -kT\ln(\nu_0 t)$ (curve with symbol ●). It can

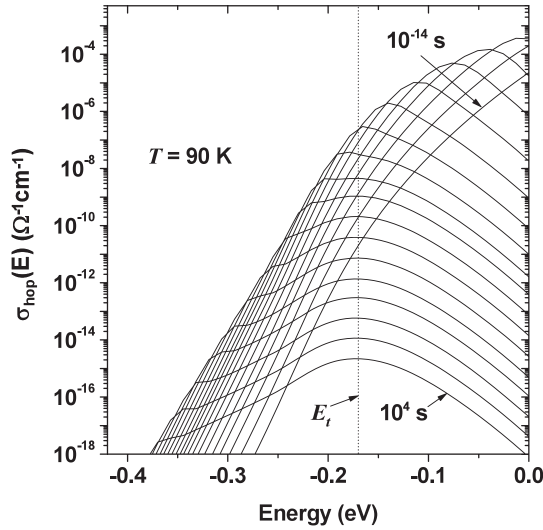

Figure 5. Energy distribution of the EH photoconductivity, $\sigma_{\mathrm{hop}}(E)$, for times ranging from 10^{-14} to 10^{4} s with a factor of 10 step and at $T = 90$ K. The transport energy E_{t} associated with the distribution peak is indicated.

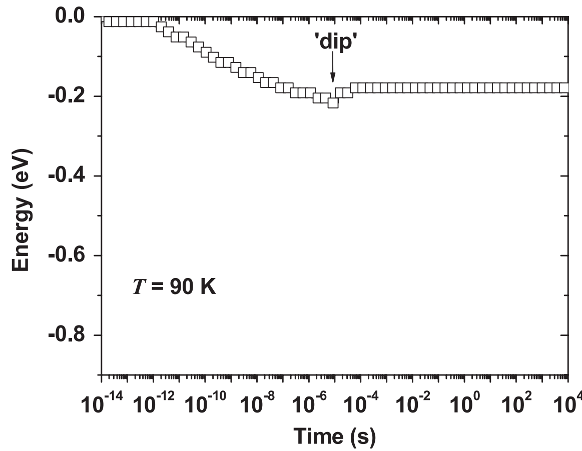

Figure 6. Time dependence of the transport energy E_{t} defined in figure 5 as the peak of the EH photoconductivity distribution.

be seen that our simulated $E_{\mathrm{d}}^{\mathrm{hop}}$-curve and its equivalent by Monroe analysis have the same form and are very close one to the other for $t > (\tau_{\mathrm{s}} = 1.5 \times 10^{-8}$ s). The only noticeable small difference between them lies in the range of time $t < \tau_{\mathrm{s}}$. This is possibly related to the Monroe approach, in which less importance was given to the role of shallower states in the hopping transport. We can also realize that the demarcation energy $E_{\mathrm{d}}^{\mathrm{hop}}$ is parallel to $E_{\mathrm{th}} = -k_{\mathrm{B}}T \ln(\nu_0 t)$ for simple MT transport for times longer than τ_{s}.

To examine the relative contribution of each of the two mechanisms, MT and EH, to the TPC, we re-plot figure 2 at two other temperatures, at low temperature ($T = 60$ K), where EH is expected to dominate the TPC, and at high temperature ($T = 300$ K), where MT is expected to be the predominant. In figure 8(a) we plot the 60 K curves of σ_{conv} (symbol $*$), σ_{ph} (symbol ○), σ_{hop} (symbol $\triangle$), and σ_{MT} (symbol $+$), where we can see clearly that MT dominates the TPC in

the range below 10^{-12} s and EH dominates above 10^{-12} s. The effect of EH on the conventional TPC σ_{conv} is well pronounced at 60 K compared to the case of 90 K (figure 2). Below 10^{-12} s trapping has not started yet for the electrons to start hopping, but as soon as trapping begins the EH takes place as the predominant mechanism ($\sigma_{hop} = \sigma_{ph}$) and the MT current component σ_{MT} falls rapidly to more than three orders of magnitude below σ_{hop}. The four photocurrents decay in parallel according to the power-law $t^{-(1-\alpha_c)}$ [3, 4]. In figure 8(b) we plot the 300 K curves of σ_{conv} (symbol ∗), σ_{ph} (symbol ○), σ_{hop} (symbol △) and σ_{MT} (symbol +). We can see clearly that EH has no effect on σ_{conv}. The MT component σ_{MT}, being superimposed on σ_{ph} and σ_{conv}, dominates the TPC over the entire simulation time range, whereas σ_{hop} is at least one order of magnitude less.

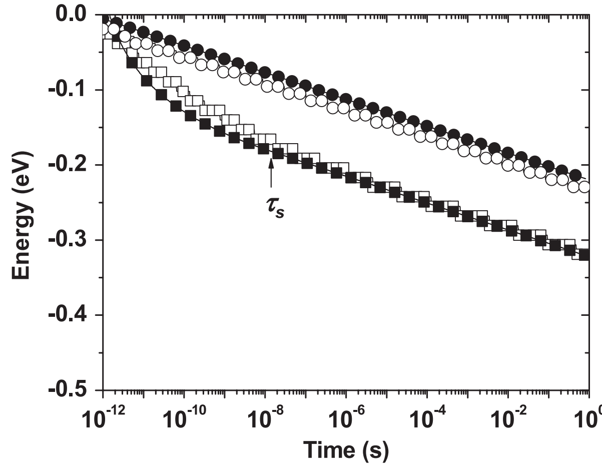

Figure 7. Time dependence of demarcation energies: □, E_d^{hop}, simulated with the presence of EH as the peak of the trapped electron density distribution in figure 4; ■, demarcation energy defined by Monroe (equations (17) and (18)), to be compared with E_d^{hop}; ○, E_d^{MT}, simulated with the absence of EH, as the peak of the trapped electron density distribution in figure 3; ●, demarcation energy $E_{th} = -k_B T \ln(\nu_0 t)$ to be compared with E_d^{MT}.

To determine the transition temperature where the TPC switches from high temperature MT transport to low temperature EH transport, we plot, in figure 9, the temperature dependence of σ_{ph} (symbol ○) and its MT and EH components, σ_{hop} (symbol △) and σ_{MT} (symbol +), at $t = 1$ μs. The time $t = 1$ μs is chosen as a good mid-value in the log timescale at which MT has already settled at high temperatures, and EH is expected to build up at the expense of MT as the temperature decreases. The curve associated with the conventional TPC, σ_{conv}, is also shown (symbol ∗) to observe its change due to EH. A clear transition can be identified around $T = 130$ K, below which the TPC switches smoothly to become EH controlled. In our previous paper on the steady state photoconductivity (SSPC) in a-Si:H with EH [8], we simulated a transition temperature from extended-state conduction to EH of about 110–120 K, which is about 10–20 K lower than the transition temperature simulated in the TPC case using the same parameters. To reconcile the two cases, we note that in the SSPC the carrier generation is continuous and the quasi-Fermi levels are close to the bands. Therefore, the density of empty states in the CBT is lower than in the TPC case where excited electrons thermalize into empty states with the dark Fermi level at mid-gap. The inter-state distance $R_{i,j}$ is then shorter in the TPC case and the hopping factor $\exp(-\frac{2R_{i,j}}{a})$ is higher, which can favor EH at higher temperatures and thus can shift up the transition temperature in the TPC compared to the SSPC.

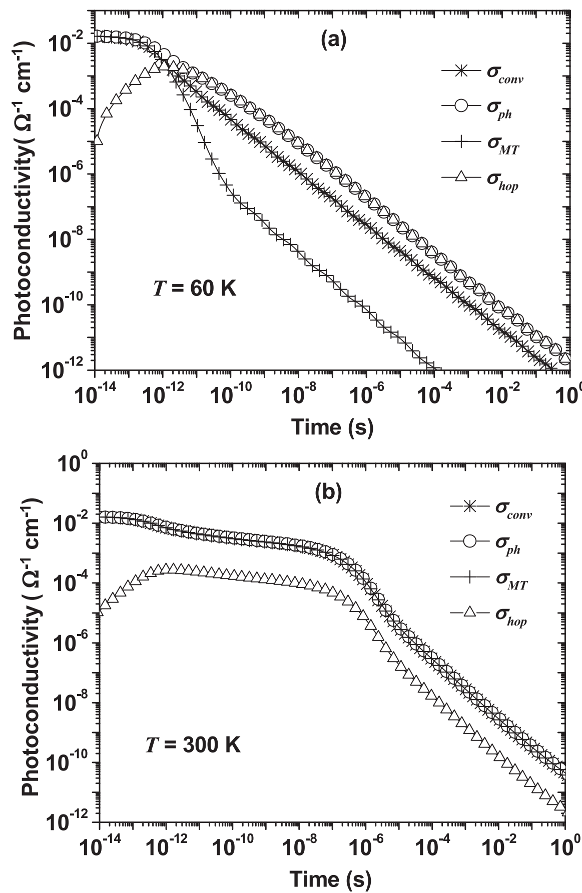

Figure 8. The TPC σ_{ph} (symbol O) and its components, MT photoconductivity σ_{MT} (symbol +) and EH photoconductivity σ_{hop} (symbol △). The conventional TPC σ_{conv} (symbol ∗) simulated without EH consideration is also shown for comparison, (a) at $T = 60$ K and (b) at $T = 300$ K.

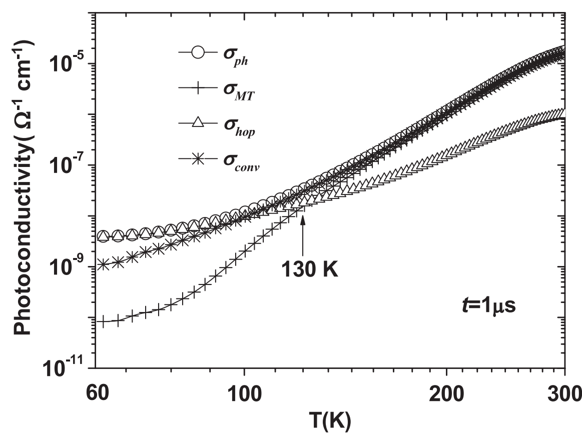

Figure 9. TPC and components as functions of temperature at $t = 1$ μs. A transition temperature around 130 K from high temperature MT transport to low temperature EH transport is determined.

4. Conclusion

The TPC in undoped a-Si:H is studied by numerical simulations at low and high temperatures in terms of a model coupling the MT and EH transports. The results are in good agreement with previous theoretical results. They provide an overall insight in which the temperature dependence of the TPC can be interpreted in terms of a transition from extended-state conduction via MT dominating at high and moderate temperatures $T > 130$ K to localized-state EH below 130 K. The predictions of Monroe analysis related to carrier thermalization and transport in exponential distribution of localized states are in good agreement with the results of our simulations, such as the EH transport energy E_t and the demarcation energy with the presence of EH E_d^{hop}.

Acknowledgments

We thank Professor C Main and Dr S Reynolds for their kind assistance with useful literature and fruitful discussions and the Algerian ministry of higher education and research for its support.

References

[1] Chittick R C, Alexander J H and Sterling H F 1969 *J. Electro-chem. Soc.* **116** 77
[2] Spear W E and Lecomber P G 1975 *Solid State Commun.* **17** 1193
[3] Tiedje T and Rose A 1980 *Solid State Commun.* **37** 49
[4] Orenstein J and Kastner M 1981 *Phys. Rev. Lett.* **46** 1421
[5] Monroe D 1985 *Phys. Rev. Lett.* **54** 146
[6] Marshall J M 2000 *Phil. Mag. Lett.* **80** 691
[7] Main C, Marshall J M and Reynolds S 2005 *J. Optoelectron. Adv. Mater.* **7** 107
[8] Merazga A, Tobbeche S, Main C, Al-Shahrani A and Reynolds S 2006 *J. Phys.: Condens. Matter* **18** 3721
[9] Powell M J and Deane S C 1993 *Phys. Rev.* B **48** 10815
[10] Powell M J and Deane S C 1996 *Phys. Rev.* B **53** 10121
[11] Okamoto H, Kida H and Hamakawa Y 1984 *Phil. Mag.* B **49** 231
[12] Main C, Berkin J and Merazga A 1991 *New Physical Problems in Electronic Materials* ed M Borissov *et al* (Singapore: World Scientific) pp 55–86
[13] Merazga A, Meftah A F, Meftah A M, Main C and Reynolds S 2001 *J. Phys.: Condens. Matter* **13** 10969
[14] Mott N F and Davis E A 1979 *Electronic Processes in Non-Crystalline Materials* (Oxford: Clarendon)
[15] Miller A and Abraham E 1960 *Phys. Rev.* **120** 745
[16] Godet C 2001 *Phil. Mag. Lett.* B **81** 205
[17] Baranovskii S D, Rubel O and Thomas P 2005 *Thin Solid Films* **487** 2–7
[18] Silver M, Schoenherr G and Baessler H 1982 *Phys. Rev. Lett.* **48** 352
[19] Marshall J M 2003 *J. Mater. Sci. Mater. Electron.* **14** 611